

Envelope vector solitons in nonlinear flexible mechanical metamaterials

A. Demiquel, V. Achilleos, G. Theocharis, and V. Tournat
*Laboratoire d'Acoustique de l'Université du Mans (LAUM), UMR 6613,
Institut d'Acoustique - Graduate School (IA-GS), CNRS, Le Mans Université, France*
(Dated: June 17, 2024)

In this paper, we employ a combination of analytical and numerical techniques to investigate the dynamics of lattice envelope vector soliton solutions propagating within a one-dimensional chain of flexible mechanical metamaterial. To model the system, we formulate discrete equations that describe the longitudinal and rotational displacements of each individual rigid unit mass using a lump element approach. By applying the multiple-scales method in the context of a semi-discrete approximation, we derive an effective nonlinear Schrödinger equation that characterizes the evolution of rotational and slowly varying envelope waves from the aforementioned discrete motion equations. We thus show that this flexible mechanical metamaterial chain supports envelope vector solitons where the rotational component has the form of either a bright or a dark soliton. In addition, due to nonlinear coupling, the longitudinal displacement displays kink-like profiles thus forming the 2-components vector soliton. These findings, which include specific vector envelope solutions, enrich our knowledge on the nonlinear wave solutions supported by flexible mechanical metamaterials and open new possibilities for the control of nonlinear waves and vibrations.

I. INTRODUCTION

Nonlinear flexible mechanical metamaterials (FlexMMs) are an emerging class of engineered materials often consisting of highly deformable soft elements connected to stiffer ones [1]. They encompass a variety of designs such as origami [2, 3] and kirigami structures [4, 5], assembled mechanical parts, 3D-printed multimaterials [6, 7], and have been shown to exhibit "exotic functionalities, such as pattern and shape transformations in response to mechanical forces, or reprogrammability" [1]. Their capacity to undergo large local deformations, including local rotations, stems from the high elasticity contrasts together with their structure and naturally implies geometric non-linearity. As with other types of metamaterials, their linear properties depend on the geometry of the structure in addition to the constituent materials, so that both non-linear and linear mechanical behaviors can be tuned by modifying their structural or material parameters. Interestingly, in the context of wave control, harnessing the nonlinear properties of a metamaterial is particularly novel, since the majority of reported results have focused on controlling linear waves by managing dispersive effects.

Despite linear wave metamaterials constitute the vast majority of studied wave control strategies, a number of nonlinear wave effects have been studied and revealed in such flexible mechanical metamaterials [8], including pulse vector solitons [9–11], rarefaction solitary waves [12, 13], transition waves and topological solitons through bistable structures for example [14–16], and more recently the manifestation of modulation instability (MI) [17].

However, to our knowledge, envelope solitons (bright and dark solitons) or breathers, have not been reported in FlexMM. Bright and dark solitons are solutions of the

universal nonlinear Schrödinger equation (NLS), and result from the complex interplay between the dispersion and nonlinearity properties of a medium [18, 19]. On the one hand bright solitons [20], are characterized by their ability to maintain a focused intensity peak during propagation. As such, these wave objects have practical applications in optical communication systems via nonlinear optical fibers, contributing to the stability and robustness of information transmission [21, 22]. On the other hand, dark solitons, which manifest themselves as stable and localized intensity drops in a wave train, have been studied in various physical contexts, including Bose-Einstein condensates in ultracold atomic gases [23], water tank experiments [24] and optics [25–27].

In terms of applications, both bright and dark solitons find utility in fields such as signal processing, optical communications, and ultrafast optics. Thus, we believe that the study of bright and dark solitons in FlexMMs will be useful in controlling large amplitude vibrations. We also expect to observe nonlinear wave phenomena in FlexMMs not yet reported in mechanics or for other wave fields. Indeed, while bright and dark solitons are mostly associated with optical systems and cold atoms, recent research has expanded their relevance to mechanical devices. For example, researchers have explored soliton-like phenomena in structures such as granular chains or phononic crystals [28, 29]. These granular solitons show potential applications in shock absorption and energy transfer mechanisms [30]. In addition, dark solitons have been studied in the context of acoustic waves with acoustic transmission lines [31], leading to the development of novel devices for sound manipulation and waveguiding [32]. The interdisciplinary study of solitons in mechanical systems reflects a growing interest and understanding of their universal properties. The applications of bright and dark solitons

in mechanical devices continue to expand, paving the way for innovations in fields such as acoustics, wave engineering, and materials science.

The main objective of this paper is to study the bright and dark soliton solutions of the NLS equation as lattice envelope vector solitons in the nonlinear FlexMM context. The paper is structured as follows. In Sec. II we present the nonlinear discrete lump model which was found to be relevant for describing the dynamical equations of FlexMMs. In section III we derive an effective NLS equation (eNLS) for the slowly varying envelope of waves of the rotational degree of freedom (DOF) in the semi-discrete approximation using asymptotic expansion and multiple-scale methods, from the discrete equations of motion of the system. Finally in sections IV and V, the existence and dynamics of bright and dark envelope vector solitons is investigated respectively.

II. LUMPED ELEMENT APPROACH

A. Problem position and modeling of the structure

The family of FlexMM that we consider in this work consists of rigid particles (in the shape of crosses) connected to their nearest neighbors by elastic connectors and periodically arranged in a chain of two rows and N columns, see Fig. 1(a). This type of structure is inspired by the FlexMM studied experimentally in ref. [10]. There, the particles are constructed with Lego[®] bricks and the elastic connectors are made with highly flexible plastic films.

To model this structure in the low-frequency regime, we adopt the lumped-element approach. We consider the particles as rigid, characterized by their mass m and their moment of inertia J , while the elastic connectors are modeled as three massless springs; a longitudinal spring with stiffness k_l , a shear spring with shear stiffness k_s , and a bending spring with bending stiffness k_θ . We focus on in-plane motion, so in general each particle has three DOFs, one rotation (around the z axis) and two displacements (one in the longitudinal direction along x and one in the transverse direction along y). We also consider only symmetric motion relative to the symmetry axis, see Fig. 1(b).

Similar to Ref. [10], we consider two DOFs, a longitudinal displacement u and a rotational motion θ . This means that we constrain the particles not to move along the y -axis. Ignoring the transverse motion may also be valid even without this forced constraint. In fact, for the structure of Ref. [10] it was shown numerically and experimentally that during the soliton propagation [9, 10], ignoring the transversal displacement is a reasonable assumption, since the transversal displacement amplitude was experimentally found to be an order of magnitude smaller than the longitudinal one.

The sign of the rotation angles is considered positive in

the trigonometric direction. In previous works [10, 17], the angle is defined as a positive-negative alternation from one cell to the next, which is a different point of view but does not change the physics. The choice made here makes the analysis easier, since we are studying modulated waves.

B. Motion equations of the system

Based on the previous assumptions, we can establish the governing equations of a one-dimensional chain starting with perfect initial alignment, resulting in a static angle of zero. Considering a single element (a cross), the position of its extremities are,

$$\begin{aligned} \mathbf{r}_1 &= \begin{pmatrix} l \cos \theta_n \\ l \sin \theta_n \end{pmatrix} & \mathbf{r}_2 &= \begin{pmatrix} -l \sin \theta_n \\ l \cos \theta_n \end{pmatrix} \\ \mathbf{r}_3 &= \begin{pmatrix} -l \cos \theta_n \\ -l \sin \theta_n \end{pmatrix} & \mathbf{r}_4 &= \begin{pmatrix} l \sin \theta_n \\ -l \cos \theta_n \end{pmatrix}. \end{aligned} \quad (1)$$

Thanks to the position of the vertices, the elongations of horizontally oriented springs are given by,

$$\begin{aligned} \Delta \mathbf{l}_{n,1} &= \mathbf{y}_n + \{\mathbf{r}_3(\theta_{n+1}) - \mathbf{r}_3(0)\} - \{\mathbf{r}_1(\theta_n) - \mathbf{r}_1(0)\} \\ &= \begin{bmatrix} u_{n+1} - u_n - l \cos \theta_{n+1} - l \cos \theta_n + 2l \\ -l \sin \theta_{n+1} - l \sin \theta_n \end{bmatrix}, \end{aligned} \quad (2)$$

while the elongation of the vertically oriented springs is neglected, due to symmetry as mentioned above,

$$\Delta \mathbf{l}_{n,2} = \mathbf{0}. \quad (3)$$

Rotational elongation can also be expressed by,

$$\Delta \theta_{n,1} = \theta_{n+1} - \theta_n, \quad (4a)$$

$$\Delta \theta_{n-1,1} = \theta_n - \theta_{n-1}, \quad (4b)$$

$$\Delta \theta_{n,2} = 2\theta_n. \quad (4c)$$

Combining the expression of each hinge elongation, the expression for the potential energy of the system can be written,

$$\mathcal{U}_{n,p}(\Delta \mathbf{l}_{n,p}, \Delta \theta_{n,p}) = \frac{1}{2} \|\mathbf{k} \cdot \Delta \mathbf{l}_{n,p}\|^2 + \frac{1}{2} k_\theta \Delta \theta_{n,p}^2, \quad (5)$$

with, $p = \{1, 2\}$ and $\mathbf{k} = (\sqrt{k_l}, \sqrt{k_s})$. [34]

The Hamiltonian of the total system can then be

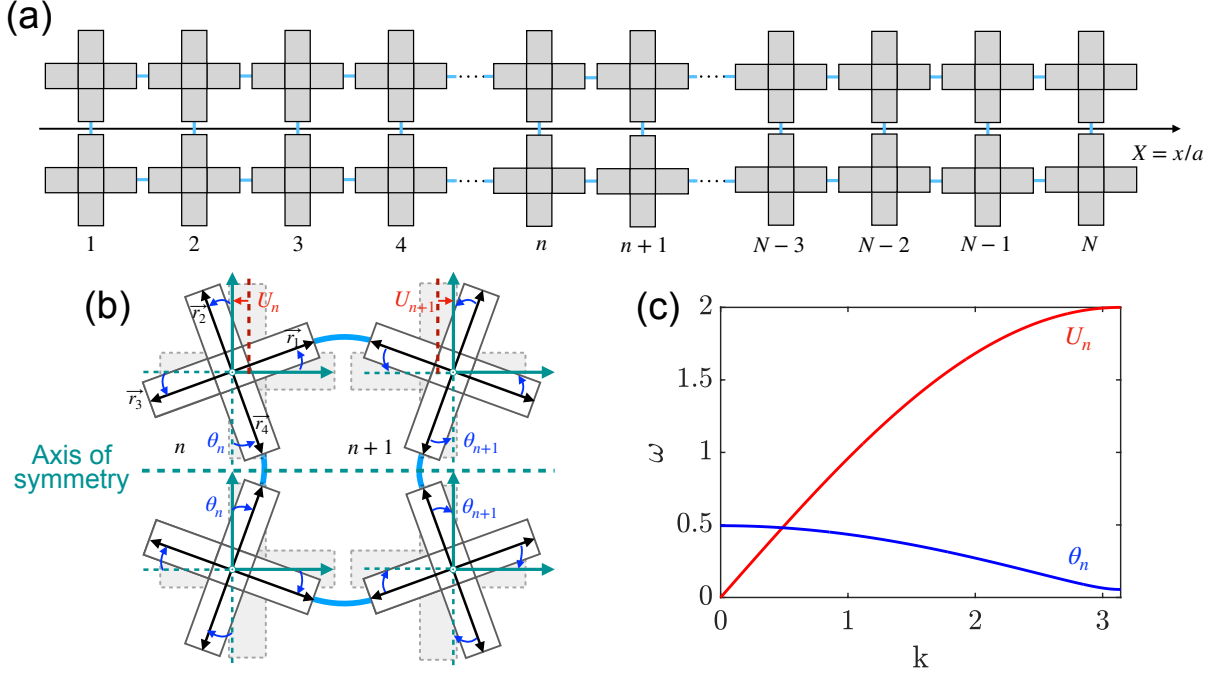


Figure 1. (a) Sketch of the FlexMM under consideration. The structure consists of two rows of rigid mass units (gray crosses) connected by elastic links (thick, blue lines) extending along the normalized X-direction ($X = x/a$) with a periodic arrangement. The rigid units are characterized by a mass m and a moment of inertia J using a normalization (cf. Eq. (8b)). The inertia of the particle can be defined by a single coefficient α . The elastic connectors are characterized by effective stiffnesses (normalized to the longitudinal spring k_l): K_s and K_θ . We consider symmetric movements relative to the horizontal axis of symmetry between the two lines. (b) Displacements of the n and $n+1$ particles from the equilibrium position, the mass units can rotate θ and longitudinally translate U . (c) Dispersion relation cf. Eq. (9) of the corresponding structure using coefficients found in the literature [10, 33]: $\alpha = 1.815$, $K_s = 0.01851$ and $K_\theta = 1.534 \cdot 10^{-4}$.

written,

$$\mathcal{H} = 2 \sum_{n=1}^N \left\{ \frac{1}{2} m \dot{u}_n^2 + \frac{1}{2} J \dot{\theta}_n^2 \right\} + 2 \sum_{n=1}^{N-1} \mathcal{U}_{n,1} (\Delta \mathbf{l}_{n,1}, \Delta \theta_{n,1}) + \sum_{n=1}^N \mathcal{U}_{n,2} (\Delta \mathbf{l}_{n,2}, \Delta \theta_{n,2}), \quad (6)$$

from which motion equations can be derived, assuming symmetry of the motions relative to the horizontal symmetry axis of the chain,

$$m \ddot{u}_n = -\frac{1}{2} \frac{\partial \mathcal{H}}{\partial u_n} = -\frac{\partial \mathcal{U}_{n-1,1}}{\partial u_n} - \frac{\partial \mathcal{U}_{n,1}}{\partial u_n}, \quad (7a)$$

$$J \ddot{\theta}_n = -\frac{1}{2} \frac{\partial \mathcal{H}}{\partial \theta_n} = -\frac{\partial \mathcal{U}_{n-1,1}}{\partial \theta_n} - \frac{\partial \mathcal{U}_{n,1}}{\partial \theta_n} - \frac{1}{2} \frac{\partial \mathcal{U}_{n,2}}{\partial \theta_n}. \quad (7b)$$

The corresponding normalized equations of motion for the n -th column are then written,

$$\frac{d^2 U_n}{dT^2} = U_{n+1} - 2U_n + U_{n-1} - \frac{\cos \theta_{n+1} - \cos \theta_{n-1}}{2}, \quad (8a)$$

$$\frac{1}{\alpha^2} \frac{d^2 \theta_n}{dT^2} = K_\theta (\theta_{n-1} - 4\theta_n + \theta_{n+1}) - K_s \cos \theta_n [\sin \theta_{n-1} + 2 \sin \theta_n + \sin \theta_{n+1}] - \sin \theta_n [2(U_{n+1} - U_{n-1}) + 4 - \cos \theta_{n-1} - 2 \cos \theta_n - \cos \theta_{n+1}], \quad (8b)$$

where we have introduced the following normalized variables and parameters: the longitudinal displacement of unit n , $U_n = u_n/a$, the normalized time $T = t\sqrt{k_l/m}$, an inertial parameter $\alpha = a\sqrt{m/(4J)}$, and stiffness parameters $K_\theta = 4k_\theta/(k_l a^2)$ and $K_s = k_s/k_l$. Above, m and J are the mass and the moment of inertia of the rigid units, while a is the unit cell length (distance between the centers of the masses). If we compare this set of equations cf. Eq. (8) in the one used in our previous work about modulation instability [17], the connection can be made by changing the signs of angles $\theta_{n\pm 1}$.

In the linear limit, the two motion (displacements and rotations) are decoupled, i.e. each DOF follows its own dynamics, independent of the other. The corresponding

dispersion relations are given by,

$$\omega^{(1)} = 2 \sin\left(\frac{k}{2}\right), \quad (9a)$$

$$\omega^{(2)} = \pm \sqrt{4\alpha^2(K_s - K_\theta) \cos^2\left(\frac{k}{2}\right) + 6\alpha^2 K_\theta}. \quad (9b)$$

Displayed in the figure 1(c), the red branch corresponds to propagating longitudinal wave: $\omega^{(1)}$, exhibiting a typical monoatomic dispersion relation see Eq. (9a). The second branch, described by Eq. (9b), represents propagating rotational waves with an inverse Klein-Gordon type dispersion relation: $\omega^{(2)}$. Notably, this branch has

an upper cutoff frequency at $\omega_c^{(2)} = \alpha\sqrt{4K_s + 2K_\theta}$.

III. MODULATED WAVES IN FLEXMM: EFFECTIVE NLS EQUATION FROM SEMI-DISCRETE APPROXIMATION

Below we focus on weakly nonlinear solutions and consequently substitute the following expansions,

$$\cos \theta_n = 1 - \frac{\theta_n^2}{2} + \dots, \quad \sin \theta_n = \theta_n - \frac{\theta_n^3}{6} + \dots, \quad (10)$$

to Eq. (8). By keeping terms up to cubic order we end up with the following set of equations of motion,

$$\frac{d^2 U_n}{dT^2} = U_{n+1} - 2U_n + U_{n-1} - \frac{\theta_{n-1}^2 - \theta_{n+1}^2}{4}, \quad (11a)$$

$$\begin{aligned} \frac{d^2 \theta_n}{dT^2} = & -\alpha^2 (K_s - K_\theta) (\theta_{n-1} + 2\theta_n + \theta_{n+1}) - 6K_\theta \alpha^2 \theta_n + \alpha^2 (K_s - 1) \theta_n^3 - \alpha^2 \frac{\theta_n}{2} (\theta_{n-1}^2 + \theta_{n+1}^2) \\ & + \frac{\alpha^2 K_s}{6} (\theta_{n-1}^3 + 2\theta_n^3 + \theta_{n+1}^3) + K_s \alpha^2 \frac{\theta_n^2}{2} (\theta_{n-1} + \theta_{n+1}) - 2\alpha^2 \theta_n (U_{n+1} - U_{n-1}). \end{aligned} \quad (11b)$$

In order to study modulated traveling waves we make use of the semi-discrete approximation [35–37], where a carrier wave, obeying the discrete dispersion relation, is modulated by a slowly varying envelope function treated in the continuum limit. In particular, we look for solutions of the following form,

$$\begin{aligned} U_n &= \epsilon U_0 + \epsilon^2 U_2 \\ &= \epsilon G_{0,n}(T) + \epsilon^2 (G_{2,n}(T) e^{2i\sigma_n} + G_{2,n}^*(T) e^{-2i\sigma_n}), \end{aligned} \quad (12a)$$

$$\begin{aligned} \theta_n &= \epsilon \theta_1 \\ &= \epsilon (F_{1,n}(T) e^{i\sigma_n} + F_{1,n}^*(T) e^{-i\sigma_n}), \end{aligned} \quad (12b)$$

with $\sigma_n = kn - \omega T$. In this ansatz, $F_{1,n}$ is the modulation of the plane wave θ_n with phase σ_n . Also, due to the quadratic terms $\sim \theta^2$ in Eq. (11), in the ansatz for U_n we include both a dc-term $G_{0,n}$ and a term $G_{2,n}$ oscillating with a phase $2\sigma_n$. Substituting Eq. (12) into Eq. (11)(a) we arrive at the following equations collecting the dc in Eq. (13a) and $e^{2i\sigma_n}$ terms in Eq. (13b) respectively,

$$\epsilon \ddot{G}_{0,n} = \epsilon (G_{0,n-1} - 2G_{0,n} + G_{0,n+1}) - \frac{\epsilon^2}{2} (|F_{1,n-1}|^2 - |F_{1,n+1}|^2), \quad (13a)$$

$$\epsilon^2 \left(\ddot{G}_{2,n} - 4i\omega \dot{G}_{2,n} - 4\omega^2 G_{2,n} \right) = \epsilon^2 (G_{2,n-1} e^{-2ik} - 2G_{2,n} + G_{2,n+1} e^{2ik}) - \epsilon^2 \frac{F_{1,n-1}^2 e^{-2ik} - F_{1,n+1}^2 e^{2ik}}{4}. \quad (13b)$$

Similarly, substituting Eq. (12) into Eq. (11)(b) we get

the following equation collecting the $e^{i\sigma_n}$ terms,

$$\begin{aligned}
\epsilon \left[\ddot{F}_{1,n} - 2i\omega \dot{F}_{1,n} - \omega^2 F_{1,n} \right] &= \epsilon \alpha^2 (K_\theta - K_s) [F_{1,n-1} e^{-ik} + 2F_{1,n} + F_{1,n+1} e^{ik}] - \epsilon 6\alpha^2 K_\theta F_{1,n} \\
&+ \epsilon^3 3\alpha^2 (K_s - 1) |F_{1,n}|^2 F_{1,n} - \epsilon^3 \frac{\alpha^2}{2} [2F_{1,n} (|F_{1,n-1}|^2 + |F_{1,n+1}|^2) + F_{1,n}^* (F_{1,n-1}^2 e^{-2ik} + F_{1,n+1}^2 e^{2ik})] \\
&+ \epsilon^3 \frac{K_s \alpha^2}{6} [3|F_{1,n-1}|^2 F_{1,n-1} e^{-ik} + 6|F_{1,n}|^2 F_{1,n} + 3|F_{1,n+1}|^2 F_{1,n+1} e^{ik}] + \epsilon^3 \frac{K_s \alpha^2}{2} [F_{1,n}^2 (F_{1,n-1}^* e^{ik} + F_{1,n+1}^* e^{-ik}) \\
&+ 2|F_{1,n}|^2 (F_{1,n-1} e^{-ik} + F_{1,n+1} e^{ik})] - \epsilon^3 2\alpha^2 F_{1,n}^* (G_{2,n+1} e^{2ik} - G_{2,n-1} e^{-2ik}) - \epsilon^2 2\alpha^2 F_{1,n} (G_{0,n+1} - G_{0,n-1}). \tag{14}
\end{aligned}$$

We now proceed considering that the discrete functions $W_n(T) = \{F_{1,n}(T), G_{0,n}(T), G_{2,n}(T)\}$ are varying slowly in space and time. Therefore the continuum limit approximation is applied and the above discrete functions $W_n(T)$ are replaced by $W(X_1, X_2, \dots, T_1, T_2, \dots)$, where $X_i = \epsilon^i X$ and $T_i = \epsilon^i T$ are slow variables with $i = 1, 2, \dots$. Note that under this approximation the slowly varying functions are independent of the fast variables n and T . In addition $W_{n\pm 1}$, is computed up to order ϵ^2 using Taylor expansion,

$$W_{n\pm 1} = W \pm \epsilon \frac{\partial W}{\partial X_1} \pm \epsilon^2 \frac{\partial W}{\partial X_2} + \frac{\epsilon^2}{2} \frac{\partial^2 W}{\partial X_1^2} + \mathcal{O}(\epsilon^3), \tag{15}$$

and the time derivation as,

$$\dot{W}_n = \frac{\partial W}{\partial T} = \epsilon \frac{\partial W}{\partial T_1} + \epsilon^2 \frac{\partial W}{\partial T_2} + \mathcal{O}(\epsilon^3). \tag{16}$$

Substituting Eqs.(15-16) into the set of Eqs. (13-14) we arrive at a system of equations at successive orders in ϵ . The lowest order in Eq. (13a) (analogous to ϵ^3) gives us a relation between the dc-term G_0 and the envelope of the modulated plane wave F_1 ,

$$\left(\frac{\partial^2}{\partial T_1^2} - \frac{\partial^2}{\partial X_1^2} \right) G_0 = \frac{\partial |F_1|^2}{\partial X_1}. \tag{17}$$

In Eq. (13b) the lowest order is analogous to ϵ^2 and relates G_2 to F_1 as follows,

$$G_2 = \frac{i \sin(2k)}{8 (\sin^2(k) - \omega^2)} F_1^2. \tag{18}$$

We now move to Eq. (14) where at order ϵ^1 , we recover the dispersion relation,

$$\omega^2 = 4\alpha^2 (K_s - K_\theta) \cos^2 \left(\frac{k}{2} \right) + 6\alpha^2 K_\theta, \tag{19}$$

which corresponds to the branch of the rotational waves of the discrete model cf. Eq. (9b). At order ϵ^2 we obtain the solvability condition,

$$\frac{\partial F_1}{\partial T_1} + v_g \frac{\partial F_1}{\partial X_1} = 0, \tag{20}$$

where

$$v_g = - \frac{\alpha^2 (K_s - K_\theta) \sin(k)}{\omega}, \tag{21}$$

is the group velocity corresponding to Eq. (19). Up to this order F_1 is linear and not coupled to G_0, G_2 . At the order ϵ^3 we have the contribution from all fields and non-linearity, leading to the following nonlinear Schrödinger (NLS) equation,

$$i \frac{\partial F_1}{\partial \tau_2} + P \frac{\partial^2 F_1}{\partial \xi_1^2} + Q |F_1|^2 F_1 = 0, \tag{22}$$

in terms of the slow variables $\xi_1 = \epsilon(X - v_g T)$ and $\tau_2 = \epsilon^2 T$. P and Q , are the dispersion and nonlinear coefficients respectively given by the following expressions,

$$P = \frac{\alpha^2 (K_\theta - K_s) \cos(k) - v_g^2}{2\omega}, \tag{23a}$$

$$Q = \frac{1}{2\omega} \left[8K_s \alpha^2 \cos^2 \left(\frac{k}{2} \right) - \alpha^2 (5 + \cos(2k)) + \frac{\alpha^2 \sin^2(2k)}{2 (\sin^2(k) - \omega^2)} - \frac{4\alpha^2}{v_g^2 - 1} \right]. \tag{23b}$$

We note that the last two terms in Eq. (23b) arise due to the presence of G_0 and G_2 at order ϵ^3 (in the case that we consider only rotation DOF these terms are absent), and have an important effect on the resulting eNLS properties.

The NLS equation exhibits two distinct behaviors depending on the sign of the product PQ . When $PQ > 0$, it is known as focusing featuring modulational instability and bright soliton solutions among others, while for $PQ < 0$, it is referred to as defocusing with stable plane waves and dark solitons [18]. For our system the sign of PQ is determined by the choice of the carrier wavenumber k and the design characteristics of the flexible metamaterial (FlexMM) through the parameters α, K_s, K_θ [17].

In figure 2, we show the sign of PQ as a function of the wavenumber k for the fixed inertial parameter $\alpha = 1.815$ which corresponds to the experimental setup ref.[8]. In addition, we choose two different cases of bending stiffness, with very small values $K_\theta = 1.534e^{-2}$ for panels (a-c) and $K_\theta = 1.534e^{-4}$, typically found in flexible elastic metamaterials. To highlight the effect of coupling between the 2DOFs (rotation and longitudinal displacement) on the nature of NLS, in panels (a-b) we

plot the sign of the PQ product when only rotational DOF are considered, while in panels (c-d) when both DOFs are considered. Interestingly, by comparing panels (a-b) to (c-d), we observe that the coupling between the two DOFs dramatically changes the nature of the NLS. We also observe that the variation of K_s stiffness has a stronger impact in the case of 2DOFs, panels (c-d). In conclusion the nature of the eNLS crucially depends on the design characteristics of the FlexMM and the presence of 2DOFs (U_n and θ_n).

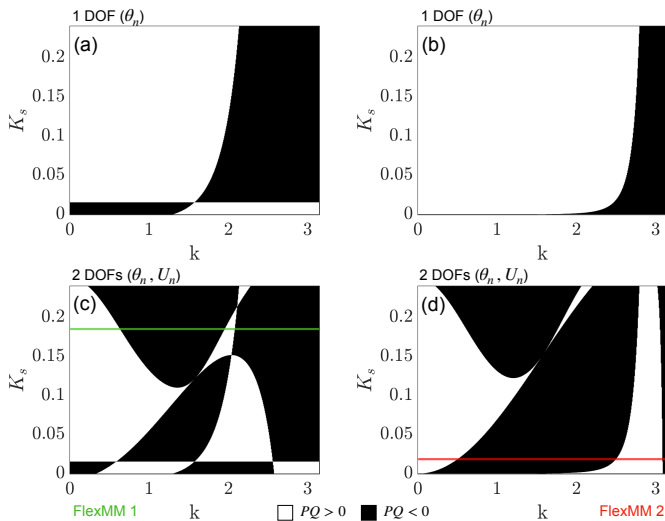


Figure 2. Sign of PQ as a function of k and K_s for two different $K_\theta = [1.534e - 2, 1.534e - 4]$ respectively used in panels (a-c) and (b-d), with $\alpha = 1.815$ fixed. Panels (a-b) correspond to a configuration where particles can only rotate, while in panels (c-d) the particles can rotate and translate. The horizontal colored lines represent the parameters chosen in Secs. IV-V to study bright and dark solitons propagation along FlexMMs.

For the rest of the paper we will focus on two particular designs of FlexMM corresponding to the green and red lines cf. Fig. 2, respectively called FlexMM 1 and FlexMM 2. In Fig. 3, we show the sign of PQ (as given by Eq. (23)) together with the dispersion relation Eq. (9) corresponding to the two FlexMM configurations mentioned above.

IV. BRIGHT ENVELOPE VECTOR SOLITONS

A. Theoretical prediction

The focusing nonlinear Schrödinger equation, Eq. (22) with $PQ > 0$, admits the following bright soliton solution [38],

$$F_1(\xi_1, \tau_2) = A_0 \operatorname{sech} \left[\frac{1}{L_e} (\xi_1 - c\tau_2) \right] e^{ic\xi_1 + iQ \left(\frac{A_0^2 - c^2}{2} \right) \tau_2}, \quad (24)$$

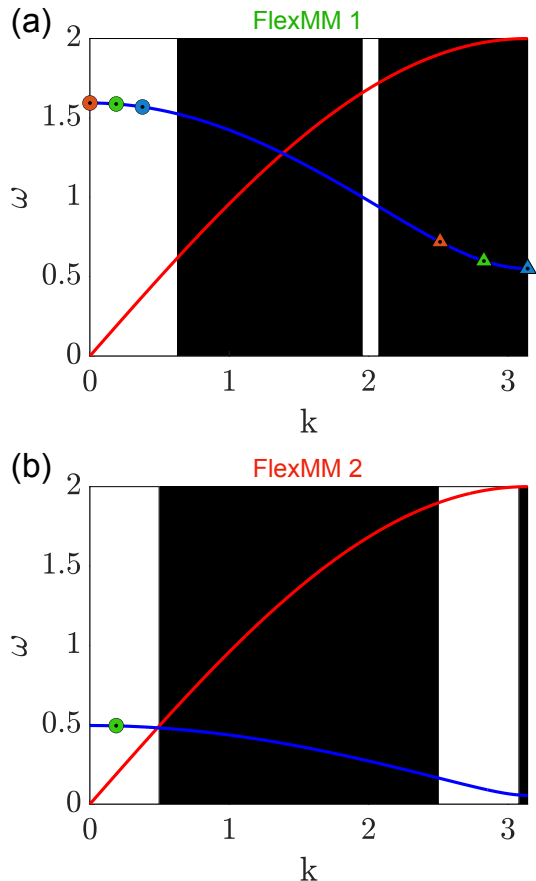


Figure 3. Dispersion relations of Eq. (8), derived in Eq. (9). The effective NLS focusing and defocusing regions are represented by white and black areas, respectively. The colored dots correspond to the pair of Ω and k used in Sec. IV to generate lattice envelope solitons. On panel (a), the dispersion relation corresponds to FlexMM 1 defined by the following set of parameters: $\alpha = 1.815$, $K_s = 0.1851$, $K_\theta = 1.534e^{-2}$. For panel (b), the FlexMM 2 parameters are: $\alpha = 1.815$, $K_s = 0.01851$, $K_\theta = 1.534e^{-4}$.

where

$$L_e = \frac{1}{A_0} \sqrt{\frac{2P}{Q}}, \quad (25)$$

is the width, A_0 the amplitude and c the velocity of the soliton at the co-moving frame coordinate system $\xi = X - v_g T$.

Using Eq. (12), the rotation θ_1 for $c = 0$ is found to be

$$\theta_1(X, T) = 2A_0 \operatorname{sech} \left[\frac{\epsilon}{L_e} (X - X_0 - v_g T) \right] \cos[kx - \Omega T]. \quad (26)$$

The angular frequency of the carrier wave,

$$\Omega = \omega^{(2)} - \epsilon^2 \frac{Q A_0^2}{2}, \quad (27)$$

has been shifted at order ϵ^2 , in comparison to the linear dispersion relation $\omega^{(2)}$ due to nonlinearity. Depending

on the sign of Q , the shift can occur above or below the linear branch.

The combination of Eqs. (24) and (17) gives the following expression for the dc-term,

$$U_0(X, T) = \frac{A_0^2 L_e}{v_g^2 - 1} \tanh \left[\frac{\epsilon(X - X_0) - \epsilon v_g T}{L_e} \right]. \quad (28)$$

Equations (26) and (28) constitute a polarized envelope nonlinear wave solution of Eq. (8) which is propagating with a common velocity determined by the spatial frequency of the carrier wave, defined as $v_g = \frac{d\omega^{(2)}}{dk} = -\frac{\alpha^2(K_s - K_\theta) \sin k}{\omega^{(2)}}$. From now on, we refer to it as bright envelope vector soliton (BEVS).

Note that physically this shape for the U field corresponds to a longitudinal contraction of the chain around the maximum of rotating sites during the propagation of the BEVS.

B. Bright Envelope vector soliton propagation in FlexMM

Direct numerical simulations of the discrete set of equations (8) are employed to validate our analytical predictions. The system (8) is solved using a fourth-order Runge-Kutta iterative integration scheme for a total of $N = 1000$ sites, with free boundary conditions at both ends. The results presented in section IV were obtained by performing the integration for a duration of eight nonlinear times: $t_f = 8T_{NL}$ [39]. T_{NL} is based on the initial condition (IC) amplitude A_0 , the system nonlinearity Q and the carrier wave number k cf. Eq. (23). The relationship between T_{NL} , A_0 and Q is given by,

$$T_{NL} = \frac{1}{\epsilon^2 |Q| A_0^2}. \quad (29)$$

The initial conditions are taken to be,

$$\theta(X, 0) = \epsilon \theta_1(X, 0), \quad \dot{\theta}(X, 0) = \epsilon \dot{\theta}_1(X, 0), \quad (30)$$

$$U(X, 0) = \epsilon U_0(X, 0), \quad \dot{U}(X, 0) = \epsilon \dot{U}_0(X, 0), \quad (31)$$

using Eqs. (26-28) with $X_0 = N/2 = 500$. The initial amplitude A_0 chosen for the next simulations is defined as $A_0 = A \sqrt{\frac{2P}{Q}}$ with $A = 15$. When $P = 1/2$ and $Q = 1$, $A_0 = A$ is the amplitude of the bright soliton of the normalized NLS equation. Defining the amplitude A_0 as a function of P and Q implies, from the perspective of the NLS model, that the bright soliton initial conditions for FlexMM1 and FlexMM2, represented in Figs.(4-5-7), are the same.

1. Nonlinear dynamics of FlexMM 1

We start by studying the first FlexMM structure characterized by the dispersion relation shown in Fig. 3(a), where as one can see, the upper cut-off frequencies of the two branches are close $\omega_c^{(2)} \approx \omega_c^{(1)} = 2$. We will focus on the small k region where the effective NLS is focusing and thus BEVS are predicted. In Fig. 4, we show the nonlinear dynamics of an initial condition with a BEVS with $k = 0.1885$, corresponding to the green circle point of Fig. 3(a). The dynamics confirm that indeed the IC evolves as a BEVS and propagates with a constant velocity keeping its shape undistorted in the form of an envelope for rotations θ (Fig. 4(a),(c)) and a kink for displacement U (Fig. 4(b)).

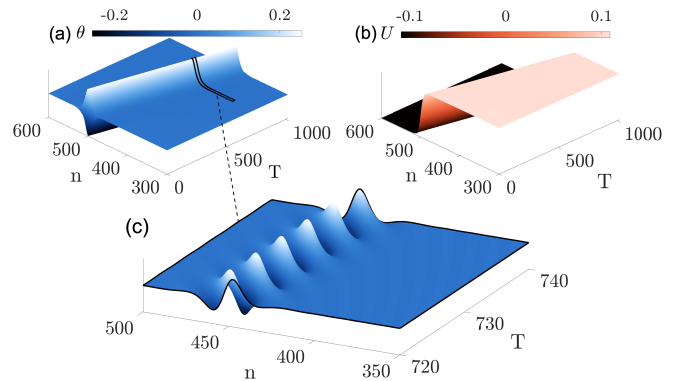


Figure 4. Evolution in time (T) of the amplitudes of the rotational (a-c) and longitudinal (b) displacements along the chain (n). The results correspond to a FlexMM (FlexMM 1) defined by the following set of parameters: $\alpha = 1.815$, $K_s = 0.1851$, $K_\theta = 1.534e^{-2}$. The initial condition corresponds to a BEVS with $k = 0.1885$ and $A = 15$, and a perturbation of $\epsilon = 0.01$.

For a more systematic study, we have performed numerical simulations of BEVS with different wavenumbers, within the focusing NLS region. In figure 5 (a-b), we show the solution profile at the final time $t_f = 8T_{NL}$ for three cases corresponding to the three circles (orange, green and blue) in Fig. 3(a). Superimposed are the theoretical solutions (black lines) given by Eqs.(26-28).

As expected, the orange one ($k = 0$) remains centered at X_0 due to $v_g = 0$, see dispersion relation curves Fig. 3(a). The other two ($k = \{0.1885, 0.3770\}$) move in the left direction due to negative group velocities, with different velocities. Overall, analytical predictions and simulation results are in good agreement. The BEVS predicted by the NLS bright soliton show a robust behavior after eight nonlinear times, confirming the validity of the effective NLS. This is a first signature that BEVs exists and propagate through the lattice. For the three cases final times of integration are close, $t_f(k = 0) \approx 1013$, $t_f(k = 0.1885) \approx 1020$, $t_f(k = 0.3770) \approx 1031$.

Another signature of the BEVS propagating through the lattice can be extracted from the nonlinear dispersion

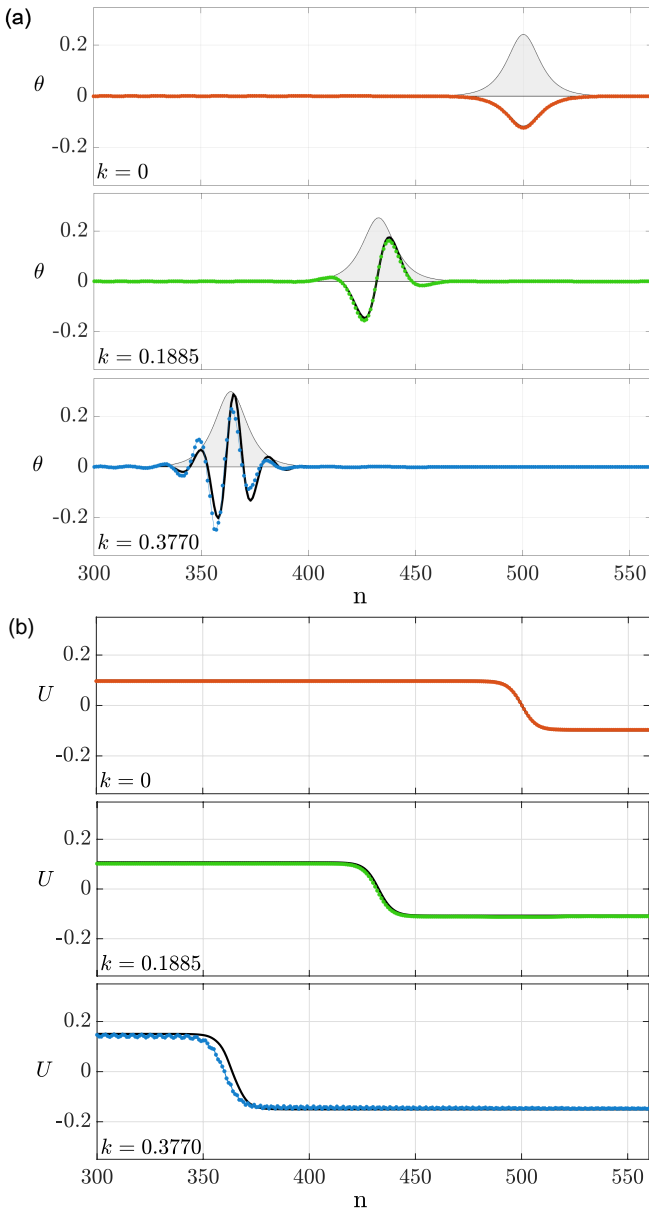


Figure 5. Rotational and longitudinal displacement amplitudes along the chain (n) at final time $t_f = 8T_{NL}$. The initial conditions correspond to BEVS with $k = 0$ in orange, $k = 0.1885$ in green and $k = 0.3770$ in blue, and an amplitude of $A = 15$, and a perturbation of $\epsilon = 0.01$.

relation (NDR). As it was shown in [40, 41], bright solitons correspond to straight lines in the NDR. To see this, let us use the space-time double Fourier transformation,

$$\tilde{\theta}_1(\omega, k) = \int_{-\infty}^{+\infty} \int_{-\infty}^{+\infty} \theta_1(X, T) e^{-ikX} e^{+i\omega T} dX dT, \quad (32)$$

using as $\theta_1(X, T)$ the BEVS solution, namely Eq. (26),

at a chosen k_s and $\omega^{(2)}(k_s)$. We obtain that,

$$\begin{aligned} \epsilon \tilde{\theta}_1(\omega, k) = & 2\pi^2 A_0 L_e \operatorname{sech} \left(\frac{\pi L_e (k - k_s)}{2\epsilon} \right) e^{-iX_0(k - k_s)} \\ & \times \delta \left(\omega_s - \frac{Q\epsilon^2 A_0^2}{2} + v_g(k - k_s) - \omega \right) \\ & + 2\pi^2 A_0 L_e \operatorname{sech} \left(\frac{\pi L_e (k + k_s)}{2\epsilon} \right) e^{-iX_0(k + k_s)} \\ & \times \delta \left(-\omega_s + \frac{Q\epsilon^2 A_0^2}{2} + v_g(k + k_s) - \omega \right). \end{aligned} \quad (33)$$

Using the Dirac function property, the value of $\delta(\omega_s - \frac{Q\epsilon^2 A_0^2}{2} + v_g(k - k_s) - \omega)$ and therefore $\tilde{\theta}_1$ is 0 except for points on the line,

$$\omega = v_g k + \left(\omega_s - v_g k_s - \epsilon^2 \frac{Q A_0^2}{2} \right). \quad (34)$$

Eq. (34) is the NDR of the BEVS which indeed is a straight line in the $\omega - k$ diagram.

Now, using the spatio-temporal dynamics, Fig. 4, we calculate the double FFT (in space and time). Since the lattice has two fields, $\theta_n(T)$ and $U_n(T)$, we apply the space-time double Fourier transform in both fields to obtain $\tilde{\theta}(\omega, k)$ and $\tilde{U}(\omega, k)$. In Fig. 6, we represented the normalized sum of the double FFT in space and time, in *log* scale,

$$\tilde{\psi}(\omega, k) = \left| \frac{\tilde{\theta}(\omega, k)}{\tilde{\theta}_{max}} \right| + \left| \frac{\tilde{U}(\omega, k)}{\tilde{U}_{max}} \right|. \quad (35)$$

As it is seen, a large amount of the 2D FFT (blue color gradient) closely matches the estimate line provided by Eq. 34, that is tangent to $\omega^{(2)}$ (yellow line) at point (Ω_s, k_s) . This corresponds to the NDR of a bright soliton. An upper shift, of the order ϵ^2 cf. Eq. (27), compared to the linear dispersion relation $\omega^{(2)}$ is visible. In addition, low frequency components around $k = 0$ are observable, on the $\omega^{(1)}$ curve. This corresponds to the dc-component of U of the BEVS solution.

2. Nonlinear dynamics of FlexMM 2

We now consider the FlexMM 2 configuration. Namely, the one that follows the dispersion relation shown in Fig. 3 (b) and which corresponds to the set of parameters used in experiments of [10, 33]. As one can see in Fig. 3 (b), this FlexMM supports rotational modes (blue curve) with frequencies that are much lower than those of the translational modes (red curve). In particular, the upper cutoff frequencies of the two branches are such that $\omega_c^{(2)} \ll \omega_c^{(1)} = 2$.

Following the same analysis as before, we now use as an initial condition Eqs. (30-31), that corresponds to a BEVS with $k = 0.1885$. The dynamics is shown in Fig. 7

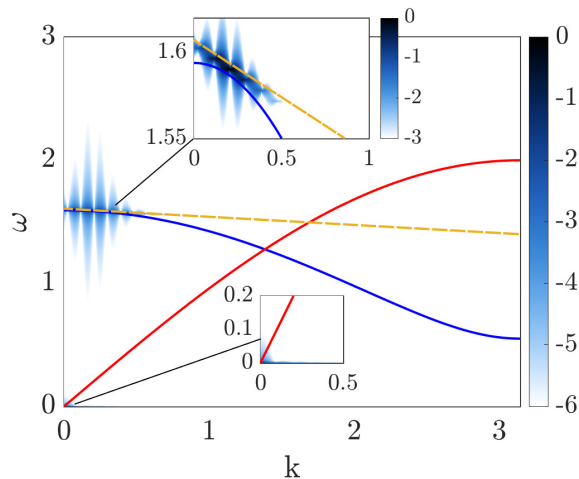


Figure 6. Numerical representation of the nonlinear dispersion relation of FlexMM 1 from its dynamics, represented in Fig. 4 using a normalized sum of the 2D-FFTs of the θ and U components. The red and blue curves denote the linear dispersion relation (see Fig. 3(a)), while the yellow line denotes NDR of the soliton described in Eq. (34). The color bar represents the $\psi(\omega, k)$, in \log scale.

The rotational dynamics is observed in panel (a), where it becomes evident that an envelope wave, in the form of a bright soliton, is propagating, accompanied by the generation of additional small waves, with frequencies around Ω_s , that are radiated by the envelope wave. Note that we have confirmed that the strength of this radiation field is of the same order as that of FlexMM 1. The latter is not visible for the scales used in Fig. 4. From the dynamics of the longitudinal displacement, see panel (b), we observe a kink profile followed by small waves, at frequency calculated to be around $2\Omega_s$, that move away at a relatively higher speed than the radiation observed in the rotation field. For a better understanding of this dynamics, we examine the temporal and spatial frequency spectra in Fig. 8.

Here, we first note that a large amount of the 2D FFT is centered around the line that is tangent to $\omega^{(2)}$ at point (Ω_s, k_s) . This corresponds to the NDR of a bright soliton. We also note that again we have spectral contribution around $k = 0$, coming from the dc-term, cf. Eq. (34). These two observations are a signature of the BEVS propagation through the lattice. However, in this case we also observe significant components of the 2D FFT in other regimes of the $\omega - k$ space. In particular, we observe frequencies around $2\Omega_s$ belonging to the dispersion of the U DOF i.e., $\omega^{(1)}$ (see rightmost inset of Fig. 8) as expected by the quadratic terms in Eq. (11a). These frequency components corresponding to the radiation field of U . Note that this was not the case for FlexMM 1, since this frequency was in the gap of the corresponding dispersion relation.

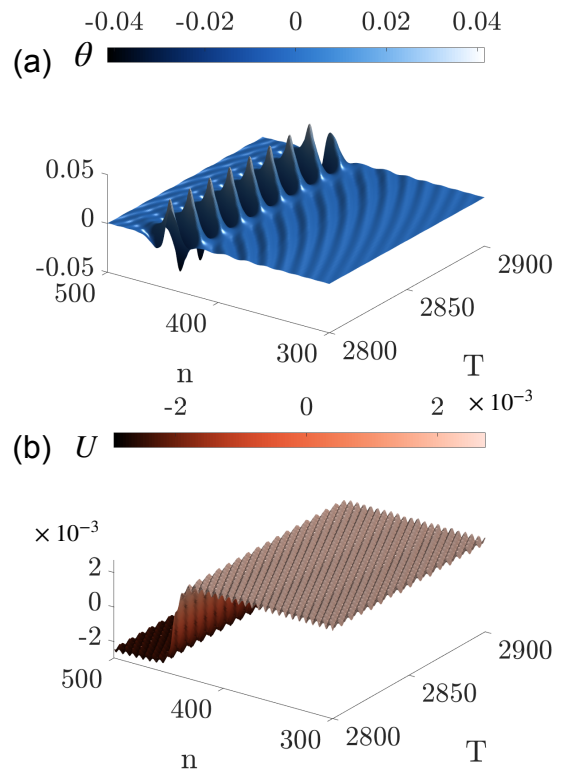


Figure 7. Evolution in time (T), for a duration between $T=[2800; 2900]$, of the amplitudes of rotational (a) and longitudinal (b) displacements along the chain (n), zoomed between $n = [300; 500]$. The results correspond to a FlexMM (FlexMM 2) defined by the following set of parameters: $\alpha = 1.815$, $K_s = 0.01851$, $K_\theta = 1.534e^{-4}$. The bright soliton is generated by the initial conditions expressed in Eqs. (30-31) for a spatial frequency of $k = 0.1885$, an amplitude of $A = 15$, and a perturbation of $\epsilon = 0.01$.

V. DARK ENVELOPE VECTOR SOLITONS

A. Theoretical prediction

In the previous section, we studied the existence and propagation of BEVS solutions in the dispersion relation region corresponding to the focusing eNLS equation, $PQ > 0$. Let us now turn our attention to the regions associated with a defocusing eNLS, where $PQ < 0$. It is established that the defocusing eNLS admits the following dark soliton solution [38],

$$F_1(\xi_1, \tau_2) = A_0 \tanh \left[\frac{1}{L_e} (\xi_1 - \xi_0) \right] e^{-iQA_0^2 \tau_2}, \quad (36)$$

where A_0 is its amplitude and L_e is its width (see Eq. (25)). Following the steps presented in section IV, we derive the subsequent analytical solution for the rotation,

$$\theta_1(X, T) = 2A_0 \tanh \left[\frac{\epsilon}{L_e} (X - X_0 - v_g T) \right] \cos[kX - \Omega T], \quad (37)$$

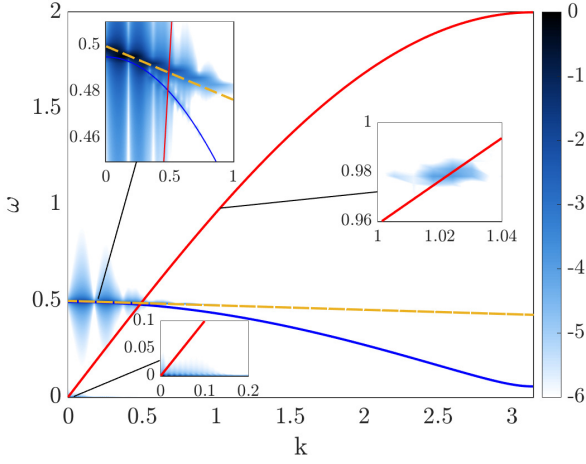


Figure 8. Numerical representation of the nonlinear dispersion relation of FlexMM 2 from its dynamics, represented in Fig. 7 using a normalized sum of the 2D-FFTs of the θ and U components. The red and blue curves denote the linear dispersion relation (see Fig. 3(b)), while the yellow line denotes NDR of the soliton described in Eq. (34). The color bar represents the $\psi(\omega, k)$, in \log scale.

where Ω is the angular frequency. Its expression is given by,

$$\Omega = \omega^{(2)} + \epsilon^2 A_0^2 Q. \quad (38)$$

As for the bright soliton solution cf. Eqs. (26-27), the angular frequency has undergone a shift at order ϵ^2 , relative to the linear $\omega^{(2)}$. This shift can manifest itself either above or below the linear branch, depending on the sign of Q . The combination of Eq. (17) with the envelope part of Eq. (37) gives an expression for G_0 yielding,

$$U_0(X, T) = \frac{A_0^2}{v_g^2 - 1} \left(\epsilon(X - X_0 - v_g T) - L_e \tanh \left[\frac{\epsilon}{L_e} (X - X_0 - v_g T) \right] \right). \quad (39)$$

Equations (37-39) form a polarized nonlinear wave solution which from now on will be called dark envelope vector soliton (DEVs).

B. Dark envelope vector soliton propagation in FlexMM

To validate our predictions regarding the existence of DEVs, we solve the discrete set of equations (8) using the process described in Sec. IV B. We apply free boundary conditions at both ends of the structure and perform the integration over a duration of five nonlinear times: $t_f = 5T_{NL}$, cf. Eq. (29).

In the case of DEVs, the presence of a jump in the phase field, see Fig. 9, leads to a mismatch with the free

boundary conditions, causing boundary effects that propagate through the lattice. To avoid these effects, similarly

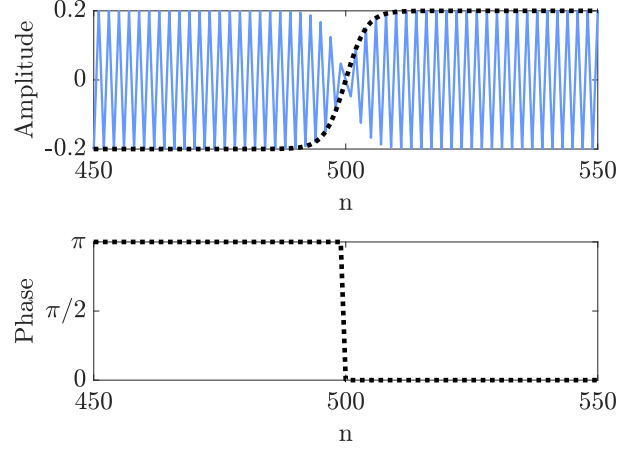


Figure 9. Analytical solution of the rotational component $e\theta_1$ (cf. Eq. (37)), and its corresponding phase at $T = 0$, for the DEVs of wave number $k = \pi$.

to [42, 43], we multiply the θ field of Eq. (37) by a super-gaussian window \mathcal{W} of the following form,

$$\mathcal{W} = e^{-\left(\frac{\xi_1 - \xi_0}{s}\right)^p} = e^{-\left(\frac{(X - X_0 - v_g T)}{s}\right)^p}, \quad (40)$$

centered on the initial position X_0 , of the dark soliton. The width of the window is governed by $s = S/\epsilon$ where the p parameter controls the edges sharpness. For the numerical simulations, we use $s = N/10 = 100$ and $p = 8$. The application of the spatial window \mathcal{W} modulates to zero the initial rotation displacement and velocity near the boundaries. The dependence of G_0 on F_1 established by the combination of Eqs. 24 and 17 written,

$$G_0(\xi_1) = \frac{1}{v_g^2 - 1} \int |F_1|^2 d\xi_1, \quad (41)$$

involves that in the presence of the window \mathcal{W} , G_0 is now dependent on the product $F_1 \mathcal{W}$. Substituting F_1 by $F_1 \mathcal{W}$ by putting Eqs. (36-40) in Eq. (41) leads to,

$$G_0(\xi_1) = \frac{A_0^2}{v_g^2 - 1} \int \tanh^2 \left(\frac{\xi_1 - \xi_0}{L_e} \right) e^{-2\left(\frac{\xi_1 - \xi_0}{s}\right)^p} d\xi_1. \quad (42)$$

The resulting integral has no analytical solution. Thus, the integration is numerically solved by computing the approximate cumulative integral of Eq. (42) via the trapezoidal method for each time step of the integration. At $T = 0$ the result gives the initial condition Eq. (43c). Performing the derivative on real time (T), noted $(\dot{})$, before the numerical integration allows to obtain the initial condition for the velocity Eq. (43d). Finally, the initial conditions employed to excite the lattice are,

$$\theta(X, 0) = \epsilon \theta_1(X, 0) \mathcal{W}(X, 0), \quad (43a)$$

$$\dot{\theta}(X, 0) = \epsilon \dot{\theta}_1(X, 0) \mathcal{W}(X, 0) + \dots, \quad (43b)$$

$$U(\xi_1, 0) = \frac{\epsilon}{v_g^2 - 1} \int |F_1|^2 \mathcal{W}^2 d\xi_1, \quad (43c)$$

$$\dot{U}(\xi_1, 0) = \frac{\epsilon}{v_g^2 - 1} \int |F_1|^2 \dot{\mathcal{W}}^2 d\xi_1 + \dots \quad (43d)$$

The $\dot{\mathcal{W}}$ terms in Eqs. (43b - 43d) can be neglected because they are proportional to ϵ^p . Moreover in the numerical simulations $\dot{\mathcal{W}}$ is proportional to ϵ^8 .

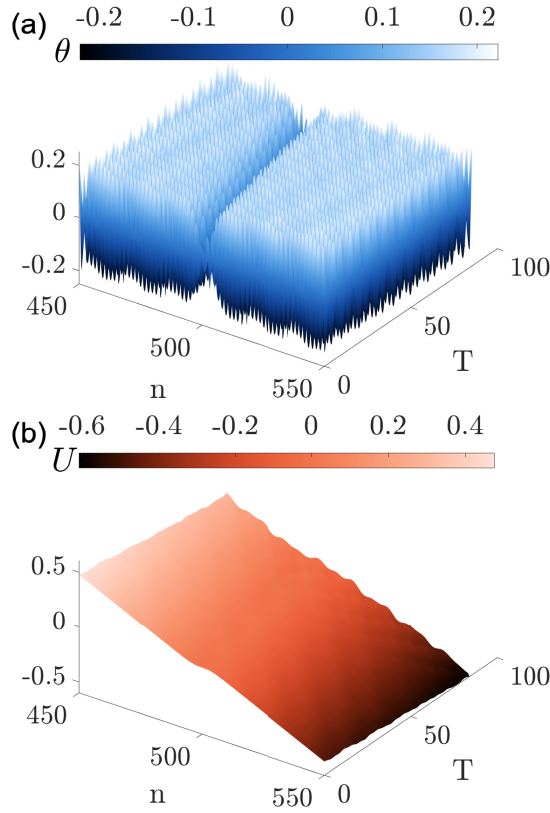


Figure 10. Panels (a-b) represent the evolution in time (T) of the rotational (a) and longitudinal (b) displacements along the chain (n). The results correspond to a FlexMM (FlexMM 1) defined by the following set of parameters : $\alpha = 1.815$, $K_s = 0.1851$, $K_\theta = 1.534e^{-2}$. A DEVS is generated by the initial conditions expressed in Eqs. (30-31), for a spatial frequency of $k = 2.9531$, and an amplitude of $\epsilon A_0 = 0.1$.

In Fig. 10, we show the nonlinear dynamics of the FlexMM 1, cf. Fig. 3(a) using as an initial condition a DEVS (Eq. 43) with $k = 2.9531$ (see green triangle in Fig. 3(a)). As one can see in Fig. 10(a), the envelope of the rotational DOF is a continuous dip that propagates at a constant velocity and maintains its shape. Moreover, the profile of U , displayed in Fig. 10(b), also remains approximately constant in time, which is a characteristic of

vector solitary waves according to our theoretical predictions. To complete the analysis, Fig. 11 represents DEVS at final time of integration in FlexMM 1 for initial conditions with different wave numbers indicated by colored triangles in Fig. 3(a). We can see that the numerical results (color dotted lines) remain close to the theoretical ones, in terms of the carrier wave (black line) and of the absolute value of the envelope (gray area).

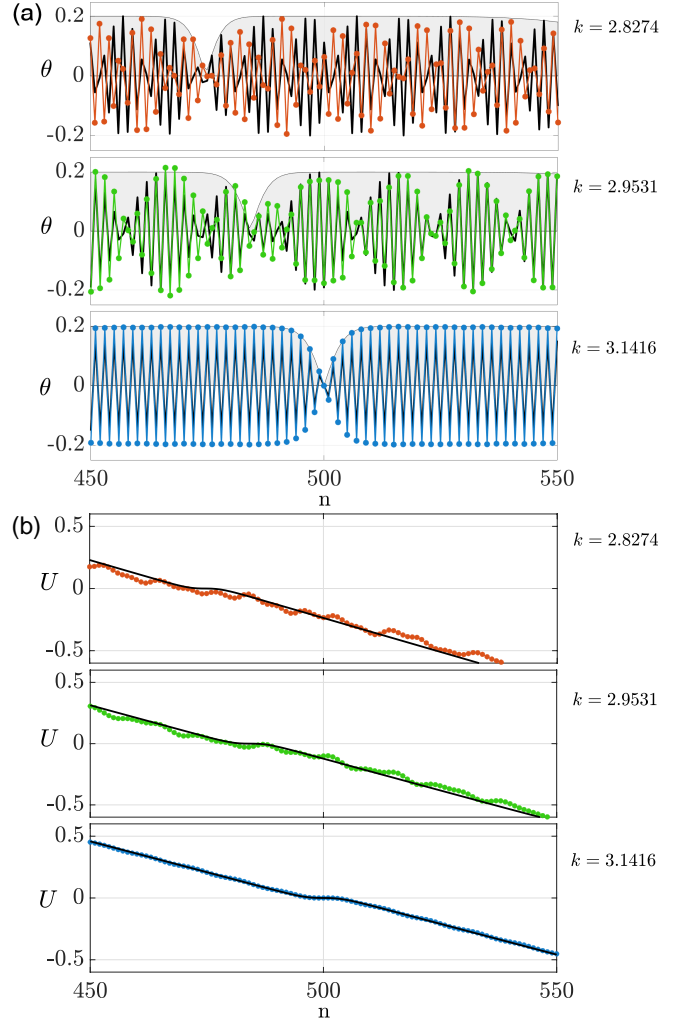


Figure 11. Rotational and longitudinal displacement amplitudes along the chain (n) at final time $t_f = 5T_{NL}$. The DEVS are generated by initial conditions : a spatial frequency of $k = 2.8274$ in orange , $k = 2.9531$ in green, and $k = \pi$ in blue. For the three cases an amplitude of $A_0 = 10$ and a perturbation of $\epsilon = 0.01$ are used.

VI. CONCLUSION

In our study, FlexMMs are mechanical structures with special properties, such as geometric nonlinearity resulting from the rotation of their constituent particles. The presence of multiple DOFs and the remarkable tunability

of their components provide an ideal experimental platform for the study of various nonlinear wave phenomena. In this work, we demonstrated the generation and propagation of nonlinear envelope waves under the form of bright and dark envelope vector solitons. In particular, we found that the rotational DOF can be described by an eNLS equation, and that longitudinal displacements follow the dynamics induced by the nonlinear coupling through a dc-term at the leading order. This dc-term was not observed in our studies on modulation instability phenomena [17]. Both analytical and numerical results show that with an appropriate choice of physical parameters for the FlexMM, in particular specific combinations of inertia α and stiffness parameters (K_s and K_θ), the propagation of these solutions in FlexMMs becomes feasible and robust. This demonstrates the significant versatility offered by the proposed system in the manipulation of weakly nonlinear modulated waves.

The present work demonstrates the great potential

that nonlinear FlexMMs have for the observation and control of both typical and novel nonlinear phenomena related to modulated waves. Several natural extensions of this work include the excitation of the system using driving functions on one of the extremity of the chain, as well as adding dissipation in the system using for example linear viscous damping terms in the discrete set of equations of motion. Both aspects are currently under investigation and results will be presented in future publications with experimental results. Other interesting perspectives are the generation and dynamics of coherent structures such as the Peregrine soliton [44], breathers or extreme wave [45, 46] effects in nonlinear FlexMMs.

ACKNOWLEDGEMENT

The authors acknowledge the support from the project ExFLEM ANR-21-CE30-0003-01.

-
- [1] K. Bertoldi, V. Vitelli, J. Christensen, and M. van Hecke, Flexible mechanical metamaterials, *Nat Rev Mater* **2**, 17066 (2017).
 - [2] E. T. Filipov, T. Tachi, and G. H. Paulino, Origami tubes assembled into stiff, yet reconfigurable structures and metamaterials, *Proc. Natl. Acad. Sci. U.S.A.* **112**, 12321 (2015).
 - [3] Y. Miyazawa, C.-W. Chen, R. Chaunsali, T. S. Gormley, G. Yin, G. Theocharis, and J. Yang, Topological state transfer in Kresling origami, *Commun Mater* **3**, 62 (2022).
 - [4] T. C. Shyu, P. F. Damasceno, P. M. Dodd, A. Lamoureux, L. Xu, M. Shlian, M. Shtein, S. C. Glotzer, and N. A. Kotov, A kirigami approach to engineering elasticity in nanocomposites through patterned defects, *Nature Mater* **14**, 785 (2015).
 - [5] M. Isobe and K. Okumura, Initial rigid response and softening transition of highly stretchable kirigami sheet materials, *Sci Rep* **6**, 24758 (2016).
 - [6] J. R. Raney and J. A. Lewis, Printing mesoscale architectures, *MRS Bull.* **40**, 943 (2015).
 - [7] S. Sundaram, M. Skouras, D. S. Kim, L. Van Den Heuvel, and W. Matusik, Topology optimization and 3D printing of multimaterial magnetic actuators and displays, *Sci. Adv.* **5**, eaaw1160 (2019).
 - [8] B. Deng, J. R. Raney, K. Bertoldi, and V. Tournat, Nonlinear waves in flexible mechanical metamaterials, *Journal of Applied Physics* **130**, 040901 (2021).
 - [9] B. Deng, J. R. Raney, V. Tournat, and K. Bertoldi, Elastic Vector Solitons in Soft Architected Materials, *Phys. Rev. Lett.* **118**, 204102 (2017).
 - [10] B. Deng, P. Wang, Q. He, V. Tournat, and K. Bertoldi, Metamaterials with amplitude gaps for elastic solitons, *Nat Commun* **9**, 3410 (2018).
 - [11] B. Deng, V. Tournat, P. Wang, and K. Bertoldi, Anomalous Collisions of Elastic Vector Solitons in Mechanical Metamaterials, *Phys. Rev. Lett.* **122**, 044101 (2019).
 - [12] E. B. Herbold and V. F. Nesterenko, Propagation of Rarefaction Pulses in Discrete Materials with Strain-Softening Behavior, *Phys. Rev. Lett.* **110**, 144101 (2013).
 - [13] B. Deng, Y. Zhang, Q. He, V. Tournat, P. Wang, and K. Bertoldi, Propagation of elastic solitons in chains of pre-deformed beams, *New J. Phys.* **21**, 073008 (2019).
 - [14] L. Jin, R. Khajetourian, J. Mueller, A. Rafsanjani, V. Tournat, K. Bertoldi, and D. M. Kochmann, Guided transition waves in multistable mechanical metamaterials, *Proc. Natl. Acad. Sci. U.S.A.* **117**, 2319 (2020).
 - [15] A. Zareei, B. Deng, and K. Bertoldi, Harnessing transition waves to realize deployable structures, *Proc. Natl. Acad. Sci. U.S.A.* **117**, 4015 (2020).
 - [16] H. Yasuda, L. M. Korpas, and J. R. Raney, Transition Waves and Formation of Domain Walls in Multistable Mechanical Metamaterials, *Phys. Rev. Applied* **13**, 054067 (2020).
 - [17] A. Demiquel, V. Achilleos, G. Theocharis, and V. Tournat, Modulation instability in nonlinear flexible mechanical metamaterials, *Phys. Rev. E* **107**, 054212 (2023).
 - [18] M. J. Ablowitz, B. Prinari, and A. D. Trubatch, *Discrete and Continuous Nonlinear Schrodinger Systems*, cambridge university press ed. (2004).
 - [19] M. Peyrard and T. Dauxois, *Physics of solitons*, in *Physics of solitons* (2010) cambridge university press ed., pp. 71–109.
 - [20] Y. Silberberg, Collapse of optical pulses, *Opt. Lett.* **15**, 1282 (1990).
 - [21] A. Hasegawa and F. Tappert, Transmission of stationary nonlinear optical pulses in dispersive dielectric fibers. I. Anomalous dispersion, *Appl. Phys. Lett.* **23**, 142 (1973).
 - [22] L. F. Mollenauer, R. H. Stolen, and J. P. Gordon, Experimental Observation of Picosecond Pulse Narrowing and Solitons in Optical Fibers, *Phys. Rev. Lett.* **45**, 1095 (1980).
 - [23] L. Pitaevskii and S. Stringari, *Bose-Einstein condensation and superfluidity*, Vol. 164 (Oxford University Press., 2016).

- [24] A. Chabchoub, O. Kimmoun, H. Branger, N. Hoffmann, D. Proment, M. Onorato, and N. Akhmediev, Experimental Observation of Dark Solitons on the Surface of Water, *Physical Review Letters* **110**, 124101 (2013).
- [25] P. Emplit, J. Hamaide, F. Reynaud, C. Froehly, and A. Barthelemy, Picosecond steps and dark pulses through nonlinear single mode fibers, *Optics Communications* **62**, 374 (1987).
- [26] D. Krökel, N. J. Halas, G. Giuliani, and D. Grischkowsky, Dark-Pulse Propagation in Optical Fibers, *Phys. Rev. Lett.* **60**, 29 (1988).
- [27] A. M. Weiner, J. P. Heritage, R. J. Hawkins, R. N. Thurston, E. M. Kirschner, D. E. Leaird, and W. J. Tomlinson, Experimental Observation of the Fundamental Dark Soliton in Optical Fibers, *Phys. Rev. Lett.* **61**, 2445 (1988).
- [28] C. Chong, P. G. Kevrekidis, G. Theocharis, and C. Daraio, Dark breathers in granular crystals, *Phys. Rev. E* **87**, 042202 (2013).
- [29] C. Chong, F. Li, J. Yang, M. O. Williams, I. G. Kevrekidis, P. G. Kevrekidis, and C. Daraio, Damped-driven granular chains: An ideal playground for dark breathers and multibreathers, *Phys. Rev. E* **89**, 032924 (2014).
- [30] V. F. Nesterenko, Waves in strongly nonlinear discrete systems, *Phil. Trans. R. Soc. A* **376**, 20170130 (2018).
- [31] J. Zhang, V. Romero-García, G. Theocharis, O. Richoux, V. Achilleos, and D. Frantzeskakis, Dark Solitons in Acoustic Transmission Line Metamaterials, *Applied Sciences* **8**, 1186 (2018).
- [32] G. Theocharis, N. Boechler, and C. Daraio, Nonlinear Periodic Phononic Structures and Granular Crystals, in *Acoustic Metamaterials and Phononic Crystals*, Vol. 173, edited by P. A. Deymier (Springer Berlin Heidelberg, Berlin, Heidelberg, 2013) pp. 217–251, series Title: Springer Series in Solid-State Sciences.
- [33] X. Guo, Nonlinear architected metasurfaces for acoustic wave scattering manipulation, Acoustics [physics.class-ph], Université du Maine (2018), nNT : 2018LEMA1030.
- [34] Note that this model for the elastic potential energy assumes that the elastic bonds between vertices behave physically in the following way: the bending/rotational restoring moment just depends on the relative angles between the neighboring units, the shear restoring force is proportional to the elongation of the connector projected on the axis orthogonal to the connector axis at rest (e.g. a vertical displacement difference of the vertices for a horizontal connector), and the longitudinal restoring force is proportional to the elongation of the connector projected on the axis of the connector axis at rest. A more general model could be implemented, accounting for global rotation effects and geometrical nonlinearity associated to large rotations, but would not necessarily lead to tractable motion equations. These assumptions have been previously experimentally validated for soliton propagation in similar metamaterial chains [8, 10, 11].
- [35] Y. S. Kivshar and M. Peyrard, Modulational instabilities in discrete lattices, *Phys. Rev. A* **46**, 3198 (1992).
- [36] I. Daumont, T. Dauxois, and M. Peyrard, Modulational instability: first step towards energy localization in nonlinear lattices, *Nonlinearity* **10**, 617 (1997).
- [37] M. Remoissenet, Low-amplitude breather and envelope solitons in quasi-one-dimensional physical models, *Phys. Rev. B* **33**, 2386 (1986).
- [38] Y. S. Kivshar and G. Agrawal, *Optical Solitons: From Fibers to Photonic Crystals*, 1st ed. (Academic Press, 2003).
- [39] M. Remoissenet, *Waves Called Solitons*, Advanced Texts in Physics (Springer Berlin Heidelberg, Berlin, Heidelberg, 1999).
- [40] A. Tikan, F. Bonnefoy, G. Ducrozet, G. Prabhudesai, G. Michel, A. Cazaubiel, É. Falcon, F. Copie, S. Randoux, and P. Suret, Nonlinear dispersion relation in integrable turbulence, *Sci Rep* **12**, 10386 (2022).
- [41] K. P. Leisman, D. Zhou, J. W. Banks, G. Kovačič, and D. Cai, Effective dispersion in the focusing nonlinear Schrödinger equation, *Phys. Rev. E* **100**, 022215 (2019).
- [42] D. J. Frantzeskakis, Dark solitons in atomic Bose–Einstein condensates: from theory to experiments, *J. Phys. A: Math. Theor.* **43**, 213001 (2010).
- [43] R. Zaera, J. Vila, J. Fernandez-Saez, and M. Ruzzene, Propagation of solitons in a two-dimensional nonlinear square lattice, *International Journal of Non-Linear Mechanics* **106**, 188 (2018).
- [44] A. Tikan, C. Billet, G. El, A. Tovbis, M. Bertola, T. Sylvestre, F. Gustave, S. Randoux, G. Genty, P. Suret, and J. M. Dudley, Universality of the Peregrine Soliton in the Focusing Dynamics of the Cubic Nonlinear Schrödinger Equation, *Phys. Rev. Lett.* **119**, 033901 (2017).
- [45] E. G. Charalampidis, J. Lee, P. G. Kevrekidis, and C. Chong, Phononic rogue waves, *Phys. Rev. E* **98**, 032903 (2018).
- [46] A. Tikan, S. Randoux, G. El, A. Tovbis, F. Copie, and P. Suret, Local Emergence of Peregrine Solitons: Experiments and Theory, *Front. Phys.* **8**, 599435 (2021).